



Detection of *EGFR* mutations in early-stage lung adenocarcinoma by machine learning-based radiomics

Kenshiro Omura^{1#}, Yu Murakami^{2,3#}, Kohei Hashimoto¹, Hikaru Takahashi², Ryoko Suzuki³, Yasuo Yoshioka³, Masahiko Oguchi^{2,3}, Junji Ichinose¹, Yosuke Matsuura¹, Masayuki Nakao¹, Sakae Okumura¹, Mingyon Mun¹

¹Department of Thoracic Surgical Oncology, the Cancer Institute Hospital, Japanese Foundation for Cancer Research, Tokyo, Japan; ²AI Medical Center, the Cancer Institute Hospital, Japanese Foundation for Cancer Research, Tokyo, Japan; ³Radiation Oncology Department, the Cancer Institute Hospital, Japanese Foundation for Cancer Research, Tokyo, Japan

Contributions: (I) Conception and design: K Hashimoto, Y Murakami; (II) Administrative support: M Mun; (III) Provision of study materials or patients: K Omura, K Hashimoto, Y Murakami, H Takahashi; (IV) Collection and assembly of data: K Omura, K Hashimoto, Y Murakami, H Takahashi, R Suzuki; (V) Data analysis and interpretation: K Omura, K Hashimoto, Y Murakami, H Takahashi, R Suzuki; (VI) Manuscript writing: All authors; (VII) Final approval of manuscript: All authors.

[#]These authors contributed equally to this work.

Correspondence to: Kohei Hashimoto, MD, PhD. Department of Thoracic Surgical Oncology, the Cancer Institute Hospital, Japanese Foundation for Cancer Research, 3-8-31 Ariake, Koto, Tokyo 135-8550, Japan. Email: kohei.hashimoto@jfcf.or.jp.

Background: We hypothesized that epidermal growth factor receptor (*EGFR*) mutations could be detected in early-stage lung adenocarcinoma using radiomics.

Methods: This retrospective study included consecutive patients with clinical stage I/II lung adenocarcinoma who underwent curative-intent pulmonary resection from March–December 2016. Using preoperative enhanced chest computed tomography, 3,951 radiomic features were extracted in total from the tumor (area within the tumor boundary), tumor rim (area within ± 3 mm of the tumor boundary), and tumor exterior (area between +10 mm outside the tumor and tumor boundary). A machine learning-based radiomics model was constructed to detect *EGFR* mutations. The combined model incorporated both radiomic and clinical features (gender and smoking history). The performance was validated with five-fold cross-validation and evaluated using the mean area under the curve (AUC).

Results: Of 99 patients (mean age, 66 ± 11 years; female, 66.6%; clinical stage I/II, 89.9%/10.1%), *EGFR* mutations in the surgical specimen were detected in 46 (46.5%). A median of 4 (range, 2 to 8) radiomic features was selected for each validation session. The mean AUCs in the radiomics and combined models were 0.75 and 0.83, respectively. The two top-ranked features in the combined model were the radiomic features extracted from the tumor exterior and the tumor, indicating a higher impact of radiomic features over relevant clinical features.

Conclusions: Radiomic features, including those in the peri-tumoral area, may help detect *EGFR* mutations in lung adenocarcinomas in preoperative settings. This non-invasive image-based technology could help guide future precision neoadjuvant therapy.

Keywords: Neoadjuvant therapy; machine-learning; radiomics

Submitted Nov 22, 2022. Accepted for publication Mar 10, 2023. Published online Apr 11, 2023.

doi: 10.21037/tcr-22-2683

View this article at: <https://dx.doi.org/10.21037/tcr-22-2683>

Introduction

Molecular targeting therapy has revolutionized the landscape of the treatment of advanced-stage lung adenocarcinoma (1-5). Genetic mutations in the epidermal growth factor receptor (*EGFR*) domain are now established biomarkers to predict the treatment response using the *EGFR* tyrosine kinase inhibitor (TKI). The incidence of these mutations is approximately 50% in the Asian population and fifteen% in the Caucasian population (6). In the adjuvant settings, osimertinib, a third-generation *EGFR*-TKI, has recently been shown to prolong disease-free survival in patients with completely resected non-squamous non-small cell lung cancer (NSCLC) with *EGFR* mutations (7). Currently, the efficacy of neoadjuvant osimertinib is being tested to further improve the prognosis for resectable primary non-squamous NSCLC harboring *EGFR* mutations (8). *EGFR* mutation is also a key exclusion criterion in a clinical trial with neoadjuvant immunotherapy (Impower 30, NCT03456063). For inclusion in these clinical trials, invasive tissue biopsy is mandatory at this moment. Although computed tomography (CT)-guided biopsy can be effective in the case of peripheral lung tumors, tissue biopsy can be challenging in patients with early-stage operable lung cancers in clinical practice, where the sensitivity of the transbronchial tissue biopsy for peripheral tumors is around 57% (9) while that of the endoscopic ultrasound-guided needle aspiration of the mediastinum is around 89% (10).

Validated clinical predictors of *EGFR* mutations are reported (gender, smoking, ethnicity). A prediction model based on these three factors performed reasonably with area

under the curve (AUC) of 0.75 (11), which could be further improved. Radiomics is defined as the quantitative analysis of multiple high-throughput data derived from medical imaging examinations. Previously, radiomic features, in combination with clinical or pathological data, can be used to develop models that predict tumor characteristics in the field of lung cancers (12).

We hypothesized that *EGFR* mutations could be detected by radiomics of primary early-stage resectable lung adenocarcinoma using preoperative CT. We present the following article in accordance with the TRIPOD reporting checklist (available at <https://tcr.amegroups.com/article/view/10.21037/tcr-22-2683/rc>).

Methods

Patient selection

The study was conducted in accordance with the Declaration of Helsinki (as revised in 2013). This study was approved by the Institutional Review Board of the Cancer Institute Hospital (No. 2021-GA-1064) on June 28, 2021, and the patient consent requirement was waived because of its retrospective nature. This retrospective study included consecutive patients with clinical stage I/II lung adenocarcinoma who underwent curative-intent pulmonary resection from March 2016 to December 2016. Patients with pure ground-glass opacity or lobar atelectasis or those who received preoperative treatment were excluded. Patients who underwent only non-contrast CT or CT taken more than 2 months before surgery were also excluded. *EGFR* gene mutation status was analyzed from paraffin-embedded surgical specimens using a polymerase chain reaction (PCR) kit (cobas[®] *EGFR* Mutation Test v2, Roche, Basel, Switzerland) targeting *exons 18, 19, 20, and 21*. The overall workflow of this study is shown in *Figure 1*.

The segmentation

All patients underwent contrast-enhanced chest CT using Discovery CT750 HD (GE Healthcare, Chicago, IL, USA). The acquisition parameters were as follows: tube voltage, 120 kVp; tube current, 100–649 mA; exposure time, 400–699 ms; milliampere-seconds, 50–329.9 mAs, slice thickness, 1.25 mm (Table S1). In axial CT images under lung field view, tumor boundary was segmented into slices containing primary tumor using Eclipse software ver. 8.6 or ver. 10.0 (Varian Medical Systems, Palo Alto, CA, USA). We then

Highlight box

Key findings

- A machine learning-based model using radiomic features, extracted from the early-stage lung adenocarcinoma preoperative image, along with clinical features, predicted *EGFR* mutations with AUC of 0.83.

What is known and what is new?

- A machine learning method can help create prediction models from a large amount of extracted data and clinical features. This manuscript adds what kind of content is important for machine learning to create prediction models.

What is the implication, and what should change now?

- This non-invasive image-based technology in detecting actionable mutations may guide future precision neoadjuvant therapy.

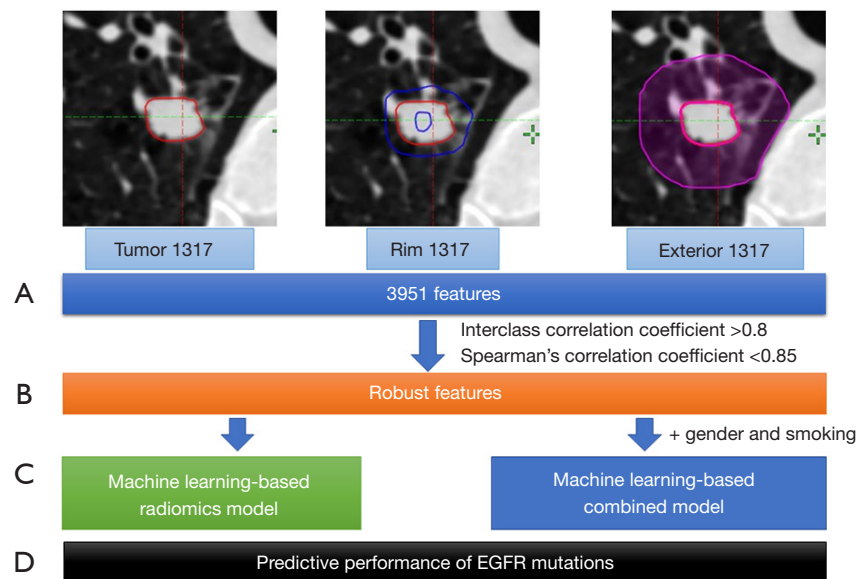


Figure 1 Study design. A: radiomic features were extracted from the preoperative enhanced CT scan. B: an interclass correlation coefficient >0.8 between two physicians was considered reproducible features. Features showing an Spearman's correlation coefficient ≥ 0.85 were excluded. C: machine learning-based models were created for prediction of EGFR mutations. D: AUC was calculated through five-fold cross-validation to evaluate predictive performance. EGFR, epidermal growth factor receptor; CT, computed tomography; AUC, area under the curve.

created volume of interests (VOIs) as follows (*Figure 1*): the tumor (VOI within the tumor boundary), tumor rim (VOI within ± 3 mm of the tumor boundary), and tumor exterior (VOI between $+10$ mm outside the tumor and the tumor boundary). The demarcation of the tumor rim and tumor exterior areas was calculated using the automated function of the software. If the created VOI went outside the lungs (i.e., the VOI partially included mediastinum or chest wall), the contour was manually modified to fit within the lung field.

The radiomics feature extraction

Prior to feature extraction, all CT images were resampled to an isotropic grid of $1 \times 1 \times 1$ mm³ using B-splines to consistently calculate the three-dimensional features. The Laplacian of Gaussian (LoG) filter ($\sigma = 0.5, 1.0, 1.5, 2.0,$ and 2.5 mm) and wavelet filter that computes eight decompositions (HHH, HHL, HLH, HLL, LHH, LHL, LLH, LLL) per level were used for transforming CT images. A total of 3,951 radiomic features, including 108 original features (first-order statistics, $n=18$; shape, $n=15$; texture, $n=75$) and 1,209 filtered features (LoG, $n=465$;

wavelet, $n=744$), were extracted from each VOI ($n=1,317 \times 3$) using PyRadiomics version 3.0.1 (13). The texture features were categorized as gray-level co-occurrence matrix ($n=24$), gray-level run length matrix ($n=16$), gray-level size zone matrix ($n=16$), gray-level dependence matrix ($n=14$), and neighboring gray-tone difference matrix ($n=5$). The bin width was set to 25 Hounsfield units (14).

The feature selection and model building

To assess the inter-observer reproducibility for VOI segmentations, segmentation of the tumor was performed using 30 randomly selected patients by two physicians with experience in lung cancer diagnostics (KH and RS) (15,16). Then, the interclass correlation coefficient (ICC) of >0.8 calculated between two physicians was considered a reproducible feature. To eliminate redundant features, Spearman's correlation coefficient (SCC) among the features of all possible two combinations was calculated, and features showing an SCC of ≥ 0.85 were excluded.

Prior to model building, each feature was standardized using Z-scores. The machine learning-based radiomics model [using the Boruta algorithm (17-19) (BorutaPy

version 0.3) for feature selection and Random Forest (Scikit-learn version 1.0.2) for prediction] was constructed to detect *EGFR* mutation. Suitable hyperparameters for Random Forest were determined by Optuna version 2.10.0 (20), while those for Boruta were empirically determined. The tuned hyperparameters by Optuna were `max_depth`, `max_leaf_nodes`, `min_samples_leaf`, and `n_estimators`. The meanings of these parameters are described in Kurasa *et al.* (17). The number of maximum iterations to select the optimal features for Boruta was set to 500. The combined model incorporated both radiomic as well as clinical features (gender and smoking history). Gender and smoking history were selected as these are clinically validated predictor of *EGFR* mutation (21). As this study was performed in monotonous population (Asians), ethnicity was not included. Other clinical variables in this study were not included to avoid overfitting. The current study is based on TRIPOD Type 1b (22).

Assessment of performance of the models and statistical analyses

The performance was validated with non-nested five-fold cross-validation, and the mean area under the receiver operating characteristic (ROC) curve was used for evaluating the prediction models. Accuracy, recall, precision, specificity, and F1 score were also calculated. Comparison of the clinical characteristics was performed for continuous and categorical variables using *t*-test or Mann-Whitney test, and Fisher's exact test, respectively. A comparison of AUCs was performed using Delong's test. Statistical analyses were performed using R software and GraphPad Prism version 8 (GraphPad Software Inc., La Jolla, CA, USA). All P values were two-sided, and $P < 0.05$ was considered statistically significant.

Results

Clinical characteristics of patients

The patient characteristics are summarized in *Table 1*. This study enrolled 99 patients (mean age, 66 ± 11 years; female, 66.6%; clinical stage I/II 89.9%/10.1%). There was no lung cancer that invaded mediastinum or chest wall. *EGFR* mutations in the surgical specimen were detected in 46 (46.5%) patients. Compared to wild type, patients with *EGFR* mutation included significantly more female (female: *EGFR* wild group, 54.7% *vs.* *EGFR* mutation

group, 78.3%; $P = 0.02$) and less smoking history (current or previous) (smoking history: *EGFR* wild group, 60.4% *vs.* *EGFR* mutation group, 19.6%; $P = 0.01$) as expected. Further, a significant difference in the histologic subtype ($P = 0.005$) between the groups existed. In the *EGFR* wild group, the most common histologic subtype was the papillary type (39.6%), followed by the solid subtype (30.2%). In the *EGFR* mutant group, the most common histologic subtype was the papillary type (71.7%), followed by the adenocarcinoma in situ (AIS)/minimally invasive adenocarcinoma (MIA) pattern (13.0%). There were no significant differences in mode of surgery and nodal status between the groups.

Among the *EGFR* mutant patients, 26 (54.2%) presented *exon 21 L858R*, 19 (39.5%) had *exon 19 deletions*, and 1 (2.1%) exhibited *exon 21 L861Q* as an uncommon mutation. Of 26 patients with *exon 21 L858R* mutation, two (4.2%) had *de novo exon 20 T790M* as well.

Feature selection and diagnostic performance

After assessing the ICC, 1,317 features extracted from VOI of the tumor were reduced to 1,267 features (in total, 3,955 features were reduced to 3,901 features). Further, 3,901 features were reduced to 453 robust radiomic features using SCC analysis (*Table S2*). Of 453 features that cleared the ICC and SCC, a median of 4 (range, 2 to 8) radiomic features from each validation session were selected using the Boruta algorithm.

The predictive performance of radiomics and combined models are summarized in *Table S3*. In the training sets, the mean AUC of the radiomics and combined models were 0.78 (range, 0.64–0.94) and 0.74 (range, 0.70–0.80), respectively. In the validation set, the combined model showed acceptable predictive performance with a mean AUC of 0.83 (range, 0.74–0.95), which tended to be higher than that of the radiomics model (mean AUC, 0.75; range, 0.65–0.82). However, Delong's test revealed that the difference in AUC did not reach statistical significance ($P = 0.052$). The ROC of each validation set in the radiomics and combined model are presented in *Figure 2*.

Importance of features selected using machine learning models

A total of 15 radiomic features from the radiomics model and 17 features, including two clinical features, from the combined model were selected through a five-fold cross-

Table 1 Clinicopathological characteristics of patients in *EGFR* wild group and *EGFR* mutation group

Variables	Total (n=99)	<i>EGFR</i> wild type (n=53)	<i>EGFR</i> mutation (n=46)	P value
Age (years)	66±11	67±10	63±11	0.06
Gender: female (%)	65 (66.6)	29 (54.7)	36 (78.3)	0.02
Smoking: yes (%)	41(41.4)	32 (60.4)	9 (19.6)	0.01
Clinical stage (%)				0.76
Stage IA	80 (80.8)	42 (79.2)	38 (82.6)	
Stage IB	9 (9.1)	4 (7.5)	5 (10.9)	
Stage IIA	4 (4.0)	3 (5.7)	1 (2.2)	
Stage IIB	6 (6.1)	4 (7.5)	2 (4.3)	
Mode of surgery (%)				0.36
Sublobar resection	14 (14.1)	9 (17.0)	5 (10.9)	
Lobectomy	83 (83.8)	42 (79.2)	41 (89.1)	
Pneumonectomy	2 (2.0)	2 (3.8)	0 (0.0)	
Pathological diagnosis (%)				0.09
pN0	83 (83.8)	43 (81.1)	40 (87.0)	
pN1	8 (8.1)	7 (13.2)	1 (2.2)	
pN2	8 (8.1)	3 (5.7)	5 (10.9)	
Histology (%)				0.005
AIS/MIA	12 (12.1)	6 (11.3)	6 (13.0)	
Papillary	54 (54.5)	21 (39.6)	33 (71.7)	
Lepidic	14 (14.1)	10 (18.9)	4 (8.7)	
Solid	19 (19.2)	16 (30.2)	3 (6.5)	

Values are presented as n (%) or mean ± SD. *EGFR*, epidermal growth factor receptor; AIS, adenocarcinoma in situ; MIA, minimally invasive adenocarcinoma; SD, standard deviation.

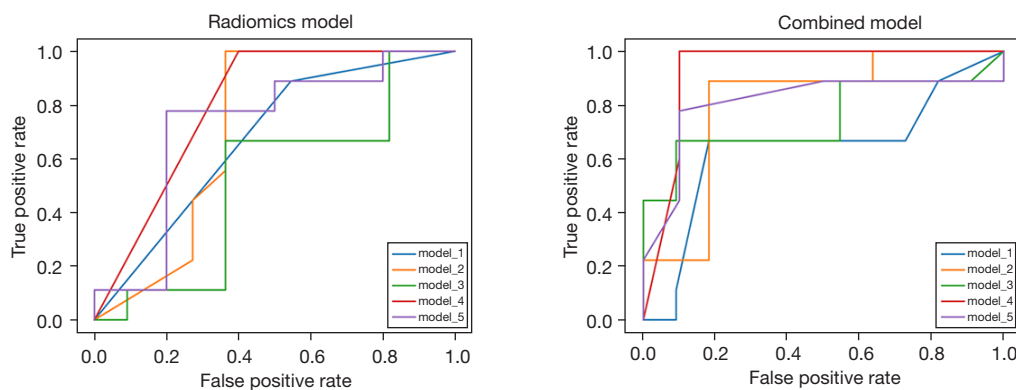


Figure 2 Receiver operating curves of each validation session in each model. The mean AUCs of five cross-validation sessions in the radiomics and combined models were 0.75 (range, 0.65–0.82) and 0.83 (range, 0.74–0.95), respectively. AUC, area under the curve.

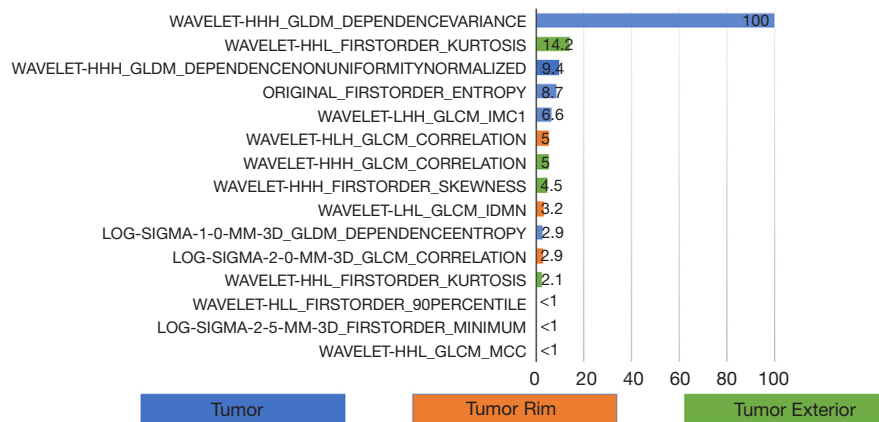


Figure 3 Ranking of features selected using Boruta algorithm in the radiomics model (each number represents a percentage of coefficient of the selected feature with reference to the top-ranked feature). HHH, HLL, HHL, LHH, LHL, HLH: wavelet filter.

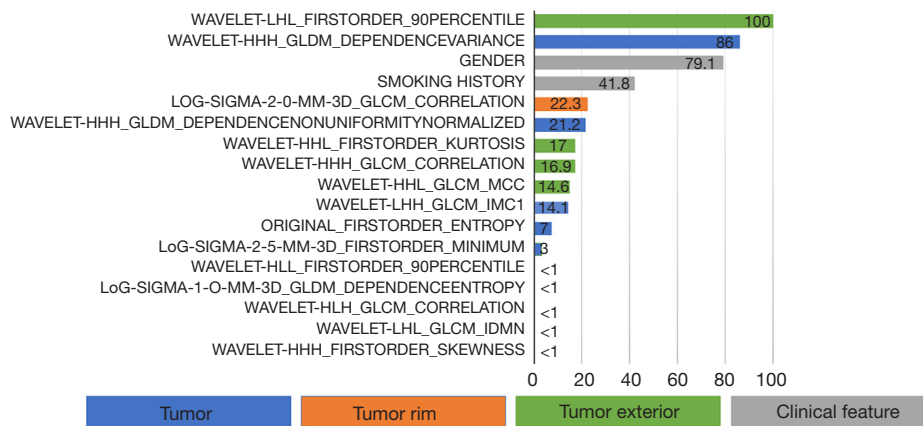


Figure 4 Ranking of features selected using Boruta algorithm in the combined model (each number represents a percentage of the coefficient of the selected feature with reference to the top-ranked feature). HHH, HHL, LHH, LHL, HLH: wavelet filter.

validation session. The selected radiomic and clinical features and the coefficients in each cross-validation session are listed in Table S4.

Figure 3 represents the ranking of each selected radiomic feature based on the average coefficient through five sessions in the radiomics model. Figure 4 shows the rankings of radiomic and clinical features in the combined model. Each feature was converted to a percentage value relative to the average coefficient of the top-ranked feature in each model. It was noted that the average coefficient of two of the radiomic features (wavelet-LHL_firstorder_90Percentile from the tumor exterior and wavelet-HHH_gldm_DependenceVariance from the tumor) were superior to

those of the relevant clinical features (gender and smoking history) in the combined model, suggesting that the radiomic features might have a higher impact on detecting *EGFR* mutations over the clinical features.

Significance of top-ranked radiomic features

Representative images showing the top three and bottom three cases in the two features that were ranked above clinical features in the combined model are demonstrated in Figure 5. The first order describes the distribution of voxel intensities within the image region. A voxel intensity of 90 percentile in the tumor exterior was selected in this feature.

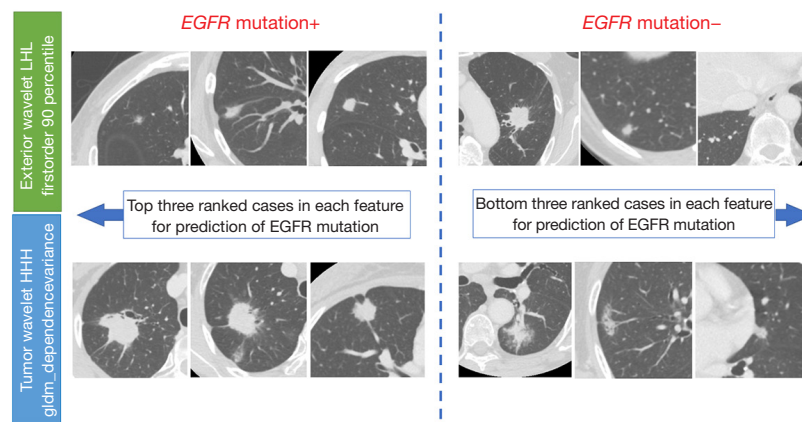


Figure 5 Left side: representative images of top three ranked cases in two radiomic features which was ranked above relevant clinical features in the combined model. Allow indicates cases with higher-ranked feature within *EGFR* mutation+. Right side: cases with bottom three ranked cases in each radiomic feature. Allow indicates cases with lower-ranked feature within *EGFR* mutation-. LHL, HHH: wavelet filter. *EGFR*, epidermal growth factor receptor.

Dependence variance measures the variance in dependence size in the image (within the tumor in this feature). No apparent recognizable pattern was observed, particularly in these images, indicating that radiomics could detect subtle changes unrecognizable to human eyes.

Discussion

In this study, we demonstrated the feasibility of predicting *EGFR* mutations in early-stage operable adenocarcinomas using radiomic features with a mean AUC of 0.75 in the validation settings. Although this was not statistically different, mean AUC improved up to 0.83 by combining with established clinical predictive factors of *EGFR* mutations (gender and smoking history). To quantify the contribution of these clinical variables more clearly, we further created the Clinical model and the all-combined model which includes all clinical variables (age, gender, smoking history, and clinical stage) and radiomic features (Table S5). Consequently, the mean AUC of the clinical model was identical to that of the radiomics model (0.77 vs. 0.75). However, the predictive performance in the all-combined model was limited (i.e., the mean AUC of 0.82), implying the selection of gender and smoking history for the Combined model is reasonable. We utilized a machine learning model to select important features and generate a predictive model out of a large number of features extracted from radiological images. Classically, the existence of air bronchogram or ground glass opacity is a known semantic

CT feature associated with *EGFR* mutations (23). However, subtle changes in the portion of ground glass opacity may not be distinguishable to the human eye. Radiomics can translate these tiny changes into the probability of mutation. Other unknown semantic or unrecognizable features, as suggested in Figure 3, were also integrated into the computation.

Previous studies have shown the possibility of *EGFR* mutation status in NSCLC utilizing CT images (24-29). However, only few of them comprised the surgical population. In this study, we focused on the preoperative CT images from early-stage NSCLC, aiming for potential usage in neoadjuvant settings. Given the ongoing research and the rapid evolution in clinical practice of advanced-stage NSCLC, as well as the adjuvant setting driven by *EGFR*-TKI (7,30) and immunotherapy (31), neoadjuvant precision medicine can plausibly become a reality with preoperative treatment guided by actionable biomarkers. *EGFR* mutation should play a pivotal role in this setting, considering its prevalence, the existence of a series of effective *EGFR*-TKIs (1-5), and its association with a low response rate to immunotherapy (32). However, biopsies for relatively small peripheral targets in early-stage operable patients can be challenging. Occasionally, the quantity or quality of samples is not enough for DNA testing. Moreover, even in the liquid biopsy (ctDNA), there is the possibility of false-negative result in NSCLC (33), thereby considering the tissue-based analysis for *EGFR* mutations as the reference standard (34). Our radiomics-based non-

invasive prediction of *EGFR* mutations could help guide the choice of preoperative treatment in this setting as additional information to the existing methods. Potentially, integration with other non-invasive predictive measures such as liquid biopsy (35) can decrease the need for biopsies in the future.

Several potential benefits of radiomic biomarkers exist in the neoadjuvant setting. First, this could avoid biopsy-related complications. Although transbronchial and trans-thoracic biopsies are considered established procedures, rare but serious complications hampering curative operations can still occur (36,37). Second, our technology could save time by skipping biopsy and waiting time for results. Waiting time before surgery can impact long-term outcomes (38); hence, saving this time could benefit patients from not just avoiding complications but also potentially improving the oncological outcomes.

Our findings suggested the importance of the peritumoral region to detect *EGFR* mutations. There are several explanations. First, the peritumoral region may have detected the skewed field of the lung parenchyma or broncho-vasculature structures, possibly due to the related mutation status of the tumor. Also, cancerous islets, known to be found adjacent to tumors (39), may be subtle changes to the human eye field but could have been detected as a radiomic feature. Second, manual demarcation may have missed some tumor edge which could have been picked as the peritumoral region. The top-ranked radiomic feature in the combined model and the second-ranked feature in the radiomics model were from the tumor exterior region, suggesting the importance of the signal outside the visible tumor margin for predicting the mutation profile.

There are several limitations to this study. First, this is a single institutional retrospective study with relatively small sample size. Although we performed cross-validation according to TRIPOD guidelines (22), our findings need further validation with a large sample set. Moreover, because it is well-known that an *EGFR* mutation profile can differ across ethnicities (40), our model may perform differently in other regions or ethnicities. Therefore, the models should be further validated in a multi-national and multi-ethnicity study. Second, although we focused only on adenocarcinomas considering the clinically proven utility of *EGFR*-TKIs against the disease and relative rarity and uncertainty of the predictive value of the treatment efficacy of squamous cell lung carcinoma *EGFR* mutation (in fact recommendation of the *EGFR* mutation testing for squamous cell carcinoma is somewhat mixed among

society guidelines), we are aware that adenocarcinoma can be confirmed only after invasive biopsy at this moment. Nevertheless, adenocarcinoma is the most relevant type of NSCLC, and this prediction model perhaps could be combined with the radiomics prediction model of the histological type of NSCLC. Besides, sometimes biopsy of a tumor only provides histology diagnosis but not enough sample for molecular testing result in daily practice. Our image biomarker may be useful in that situation. Third, we utilized manual demarcation of the tumor boundary to extract radiomic features that can be a source of errors. Although we performed ICC to diminish inter-observer variability, this could have affected the results as radiomics is sensitive to slight changes. Incorporating automated detection technology could reduce the inter-observer variation. Fourth, we chose non-nested cross validation for evaluating the prediction performance, thus optimal hyperparameters for Random Forest were not tuned using independent validation sets. Finally, we did not consider other machine-learning techniques other than Random Forest for prediction. Jia *et al.* used Random Forest classifier to predict *EGFR* mutations using radiomic features and clinical variables (29), and demonstrated that relatively higher predictive performance was observed (AUC =0.828), which is consistent with our results (AUC =0.83).

Conclusions

Radiomic features may help detect *EGFR* mutations in lung adenocarcinomas in preoperative settings. Important signals even outside the recognizable tumor boundary may exist. This non-invasive image-based technology in detecting actionable mutations could help guide future precision neoadjuvant therapy.

Acknowledgments

This paper was presented as a poster in the 102nd annual meeting of the American Association for Thoracic Surgery, Boston, MA, May 14–17, 2022.

Funding: This study was funded by the Japanese Foundation for Multidisciplinary Treatment of Cancer and the divisional funding.

Footnote

Reporting Checklist: The authors have completed the

TRIPOD reporting checklist. Available at <https://tcr.amegroups.com/article/view/10.21037/tcr-22-2683/rc>

Data Sharing Statement: Available at <https://tcr.amegroups.com/article/view/10.21037/tcr-22-2683/dss>

Peer Review File: Available at <https://tcr.amegroups.com/article/view/10.21037/tcr-22-2683/prf>

Conflicts of Interest: All authors have completed the ICMJE uniform disclosure form (available at <https://tcr.amegroups.com/article/view/10.21037/tcr-22-2683/coif>). The authors have no conflicts of interest to declare.

Ethical Statement: The authors are accountable for all aspects of the work in ensuring that questions related to the accuracy or integrity of any part of the work are appropriately investigated and resolved. The study was conducted in accordance with the Declaration of Helsinki (as revised in 2013). This study was approved by the Institutional Review Board of the Cancer Institute Hospital (No. 2021-GA-1064) on June 28, 2021, and the patient consent requirement was waived because of its retrospective nature.

Open Access Statement: This is an Open Access article distributed in accordance with the Creative Commons Attribution-NonCommercial-NoDerivs 4.0 International License (CC BY-NC-ND 4.0), which permits the non-commercial replication and distribution of the article with the strict proviso that no changes or edits are made and the original work is properly cited (including links to both the formal publication through the relevant DOI and the license). See: <https://creativecommons.org/licenses/by-nc-nd/4.0/>.

References

1. Mok TS, Wu YL, Thongprasert S, et al. Gefitinib or carboplatin-paclitaxel in pulmonary adenocarcinoma. *N Engl J Med* 2009;361:947-57.
2. Zhou C, Wu YL, Chen G, et al. Erlotinib versus chemotherapy as first-line treatment for patients with advanced EGFR mutation-positive non-small-cell lung cancer (OPTIMAL, CTONG-0802): a multicentre, open-label, randomised, phase 3 study. *Lancet Oncol* 2011;12:735-42.
3. Ramalingam SS, Vansteenkiste J, Planchard D, et al. Overall Survival with Osimertinib in Untreated, EGFR-Mutated Advanced NSCLC. *N Engl J Med* 2020;382:41-50.
4. Sequist LV, Yang JC, Yamamoto N, et al. Phase III study of afatinib or cisplatin plus pemetrexed in patients with metastatic lung adenocarcinoma with EGFR mutations. *J Clin Oncol* 2013;31:3327-34.
5. Wu YL, Cheng Y, Zhou X, et al. Dacomitinib versus gefitinib as first-line treatment for patients with EGFR-mutation-positive non-small-cell lung cancer (ARCHER 1050): a randomised, open-label, phase 3 trial. *Lancet Oncol* 2017;18:1454-66.
6. Han B, Tjulandin S, Hagiwara K, et al. EGFR mutation prevalence in Asia-Pacific and Russian patients with advanced NSCLC of adenocarcinoma and non-adenocarcinoma histology: The IGNITE study. *Lung Cancer* 2017;113:37-44.
7. Wu YL, Tsuboi M, He J, et al. Osimertinib in Resected EGFR-Mutated Non-Small-Cell Lung Cancer. *N Engl J Med* 2020;383:1711-23.
8. Tsuboi M, Weder W, Escriu C, et al. Neoadjuvant osimertinib with/without chemotherapy versus chemotherapy alone for EGFR-mutated resectable non-small-cell lung cancer: NeoADAURA. *Future Oncol* 2021;17:4045-55.
9. Rivera MP, Mehta AC, Wahidi MM. Establishing the diagnosis of lung cancer: Diagnosis and management of lung cancer, 3rd ed: American College of Chest Physicians evidence-based clinical practice guidelines. *Chest* 2013;143:e142S-65S.
10. Silvestri GA, Gonzalez AV, Jantz MA, et al. Methods for staging non-small cell lung cancer: Diagnosis and management of lung cancer, 3rd ed: American College of Chest Physicians evidence-based clinical practice guidelines. *Chest* 2013;143:e211S-50S.
11. Aye PS, Tin Tin S, McKeage MJ, et al. Development and validation of a predictive model for estimating EGFR mutation probabilities in patients with non-squamous non-small cell lung cancer in New Zealand. *BMC Cancer* 2020;20:658.
12. Lee G, Lee HY, Park H, et al. Radiomics and its emerging role in lung cancer research, imaging biomarkers and clinical management: State of the art. *Eur J Radiol* 2017;86:297-307.
13. van Griethuysen JJM, Fedorov A, Parmar C, et al. Computational Radiomics System to Decode the Radiographic Phenotype. *Cancer Res* 2017;77:e104-7.
14. Kakino R, Nakamura M, Mitsuyoshi T, et al. Application and limitation of radiomics approach to prognostic

- prediction for lung stereotactic body radiotherapy using breath-hold CT images with random survival forest: A multi-institutional study. *Med Phys* 2020;47:4634-43.
15. Nakanishi R, Akiyoshi T, Toda S, et al. Radiomics Approach Outperforms Diameter Criteria for Predicting Pathological Lateral Lymph Node Metastasis After Neoadjuvant (Chemo)Radiotherapy in Advanced Low Rectal Cancer. *Ann Surg Oncol* 2020;27:4273-83.
 16. Murakami Y, Soyano T, Kozuka T, et al. Dose-Based Radiomic Analysis (Dosiomics) for Intensity Modulated Radiation Therapy in Patients With Prostate Cancer: Correlation Between Planned Dose Distribution and Biochemical Failure. *Int J Radiat Oncol Biol Phys* 2022;112:247-59.
 17. Kursa MB, Rudnicki WR. Feature Selection with the Boruta Package. *J Stat Softw* 2010;36:1-13.
 18. Otani S, Himoto Y, Nishio M, et al. Radiomic machine learning for pretreatment assessment of prognostic risk factors for endometrial cancer and its effects on radiologists' decisions of deep myometrial invasion. *Magn Reson Imaging* 2022;85:161-7.
 19. Kursa MB. Robustness of Random Forest-based gene selection methods. *BMC Bioinformatics* 2014;15:8.
 20. Akiba T, Sano S, Yanase T, et al. A Next-generation Hyperparameter Optimization Framework. *arXiv:1907.10902v1*. 2019.
 21. Zhang YL, Yuan JQ, Wang KF, et al. The prevalence of EGFR mutation in patients with non-small cell lung cancer: a systematic review and meta-analysis. *Oncotarget* 2016;7:78985-93.
 22. Collins GS, Reitsma JB, Altman DG, et al. Transparent reporting of a multivariable prediction model for individual prognosis or diagnosis (TRIPOD): the TRIPOD statement. *BMJ* 2015;350:g7594.
 23. Cheng Z, Shan F, Yang Y, et al. CT characteristics of non-small cell lung cancer with epidermal growth factor receptor mutation: a systematic review and meta-analysis. *BMC Med Imaging* 2017;17:5.
 24. Huang Y, Liu Z, He L, et al. Radiomics Signature: A Potential Biomarker for the Prediction of Disease-Free Survival in Early-Stage (I or II) Non-Small Cell Lung Cancer. *Radiology* 2016;281:947-57.
 25. Rossi G, Barabino E, Fedeli A, et al. Radiomic Detection of EGFR Mutations in NSCLC. *Cancer Res* 2021;81:724-31.
 26. Wang S, Shi J, Ye Z, et al. Predicting EGFR mutation status in lung adenocarcinoma on computed tomography image using deep learning. *Eur Respir J* 2019;53:1800986.
 27. Liu Y, Kim J, Balagurunathan Y, et al. Radiomic Features Are Associated With EGFR Mutation Status in Lung Adenocarcinomas. *Clin Lung Cancer* 2016;17:441-448.e6.
 28. Hong D, Xu K, Zhang L, et al. Radiomics Signature as a Predictive Factor for EGFR Mutations in Advanced Lung Adenocarcinoma. *Front Oncol* 2020;10:28.
 29. Jia TY, Xiong JF, Li XY, et al. Identifying EGFR mutations in lung adenocarcinoma by noninvasive imaging using radiomics features and random forest modeling. *Eur Radiol* 2019;29:4742-50.
 30. Zhong WZ, Wang Q, Mao WM, et al. Gefitinib Versus Vinorelbine Plus Cisplatin as Adjuvant Treatment for Stage II-IIIa (N1-N2) EGFR-Mutant NSCLC: Final Overall Survival Analysis of CTONG1104 Phase III Trial. *J Clin Oncol* 2021;39:713-22.
 31. Felip E, Altorki N, Zhou C, et al. Adjuvant atezolizumab after adjuvant chemotherapy in resected stage IB-IIIa non-small-cell lung cancer (IMpower010): a randomised, multicentre, open-label, phase 3 trial. *Lancet* 2021;398:1344-57.
 32. Gainor JF, Shaw AT, Sequist LV, et al. EGFR Mutations and ALK Rearrangements Are Associated with Low Response Rates to PD-1 Pathway Blockade in Non-Small Cell Lung Cancer: A Retrospective Analysis. *Clin Cancer Res* 2016;22:4585-93.
 33. Rolfo C, Mack PC, Scagliotti GV, et al. Liquid Biopsy for Advanced Non-Small Cell Lung Cancer (NSCLC): A Statement Paper from the IASLC. *J Thorac Oncol* 2018;13:1248-68.
 34. Malapelle U, Sirera R, Jantus-Lewintre E, et al. Profile of the Roche cobas® EGFR mutation test v2 for non-small cell lung cancer. *Expert Rev Mol Diagn* 2017;17:209-15.
 35. Merker JD, Oxnard GR, Compton C, et al. Circulating Tumor DNA Analysis in Patients With Cancer: American Society of Clinical Oncology and College of American Pathologists Joint Review. *J Clin Oncol* 2018;36:1631-41.
 36. Asano F, Aoe M, Ohsaki Y, et al. Deaths and complications associated with respiratory endoscopy: a survey by the Japan Society for Respiratory Endoscopy in 2010. *Respirology* 2012;17:478-85.
 37. Tomiyama N, Yasuhara Y, Nakajima Y, et al. CT-guided needle biopsy of lung lesions: a survey of severe complication based on 9783 biopsies in Japan. *Eur J Radiol* 2006;59:60-4.
 38. Ponholzer F, Kroepfl V, Ng C, et al. Delay to surgical treatment in lung cancer patients and its impact on survival in a video-assisted thoracoscopic lobectomy cohort. *Sci Rep* 2021;11:4914.

39. Koukourakis MI, Giatromanolaki A, Thorpe PE, et al. Vascular endothelial growth factor/KDR activated microvessel density versus CD31 standard microvessel density in non-small cell lung cancer. *Cancer Res* 2000;60:3088-95.
40. Shi Y, Au JS, Thongprasert S, et al. A prospective, molecular epidemiology study of EGFR mutations in Asian patients with advanced non-small-cell lung cancer of adenocarcinoma histology (PIONEER). *J Thorac Oncol* 2014;9:154-62.

Cite this article as: Omura K, Murakami Y, Hashimoto K, Takahashi H, Suzuki R, Yoshioka Y, Oguchi M, Ichinose J, Matsuura Y, Nakao M, Okumura S, Mun M. Detection of *EGFR* mutations in early-stage lung adenocarcinoma by machine learning-based radiomics. *Transl Cancer Res* 2023;12(4):837-847. doi: 10.21037/tcr-22-2683